Journal of Energetic Materials
Publication details, including instructions for authors and subscription information:
http://www.informaworld.com/smpp/title~content=t713770432

Dissolution study of BAMO/AMMO thermoplastic elastomer for the recycling and recovery of energetic materials

Zhihua Cao[ab]; Suphan Kovenklioglu[ab]; Dilhan M. Kalyon[ab]; Rahmi Yazici[ab]
[a] Chemical Sciences and Engineering Department, Highly Filled Materials Institute, [b] Stevens Institute of Technology Castle Point on the Hudson, Hoboken, New Jersey

To cite this Article Cao, Zhihua , Kovenklioglu, Suphan , Kalyon, Dilhan M. and Yazici, Rahmi(1997) 'Dissolution study of BAMO/AMMO thermoplastic elastomer for the recycling and recovery of energetic materials', Journal of Energetic Materials, 15: 2, 73 — 107
To link to this Article: DOI: 10.1080/07370659708216075
URL: http://dx.doi.org/10.1080/07370659708216075

DISSOLUTION STUDY OF BAMO/AMMO THERMOPLASTIC ELASTOMER FOR THE RECYCLING AND RECOVERY OF ENERGETIC MATERIALS

Zhihua Cao, Suphan Kovenklioglu, Dilhan M. Kalyon and Rahmi Yazici

Chemical Sciences and Engineering Department
and Highly Filled Materials Institute

Stevens Institute of Technology
Castle Point on the Hudson, Hoboken, New Jersey 07030

ABSTRACT

This study involves the characterization and dissolution of a thermoplastic elastomer copolymer used as binder in the new generation of energetic materials. The thermoplastic binder is an oxetane based elastomer manufactured by Thiokol Corporation. Since the binder encapsulates other components in an energetic material formulation, its controlled dissolution is crucial to the recovery and recycle of all the energetic material ingredients. The polymeric binder was found to be highly soluble in ethyl acetate and THF. The dissolution rate data obtained under well defined flow dynamics was satisfactorily correlated with the film model. External mass transfer resistance was found to be generally important but became negligible for Reynolds numbers above 6.0×10^4. The mass transfer coefficients calculated on the basis of the film model were found to be an Arrhenius function of temperature. The activation energy for the dissolution rates was estimated to be 4.8 kcal/mol.

Journal of Energetic Materials Vol. 15, 73-107 (1997)
Published in 1997 by Dowden, Brodman & Devine, Inc.

INTRODUCTION

The next generation of propellants, explosives and pyrotechniques will utillize novel ingredients that are very costly including oxetane based energetic binders, ADN and CL-20 crystals. Cost as well as environmental concerns will mandate that the constituents of the energetic materials be reprocessable and recoverable. A new binder which has been developed for this purpose is the BAMO/AMMO thermoplastic elastomer manufactured by the Thiokol Corporation. The recycling and recovery process must first target the controlled dissolution of the binder since the binder encapsulates other ingredients in a typical energetic formulation. The principal focus of this study is the characterization and dissolution of BAMO/AMMO polymeric binder with varying BAMO content.

CHARACTERIZATION OF BAMO/AMMO BINDER

BAMO/AMMO thermoplastic elastomer is an alternating block copolymer obtained from the polymerization of BAMO and AMMO monomers. BAMO (3,3-bis(azidomethyl)oxetane) is a crystalline homopolymer forming the hard block and AMMO (3-azidomethyl-3-methyloxetane) is an amorphous homopolymer forming the soft block of the energetic thermoplastic elastomer.

The typical wide angle X-ray diffraction (XRD) pattern of pure BAMO polymer is shown in Figure 1 where the crystalline peaks are superimposed on an amorphous background. The analysis of these patterns revealed that pure BAMO constitutes of

45% crystalline and 55% amorphous phases at room temperature. AMMO polymer on the other hand is a viscous liquid at room temperture and is 100% amorphous according to its X-ray diffraction pattern shown in Figure 2.

The X-ray diffraction patterns of BAMO/AMMO copolymers for 25% BAMO and 18% BAMO are shown in Figures 3a and 3b, respectively. The analysis of these patterns has revealed that the BAMO polymer in these blends is only 25% crystalline, lower than the pure BAMO polymer. The addition of AMMO and BAMO apparently hinders the degree of crystallinity of the BAMO polymer. The degree of crystallinity of BAMO is expected to affect the melting and dissolution properties of the BAMO/AMMO polymer.

The differential scanning calorimetry (DSC) analysis of of pure BAMO is given in Figures 4. The melting temperature of pure BAMO is around 78 °C and the heat of fusion is 10.76 cal/g. The DSC analysis of BAMO/AMMO binder (25% BAMO) is shown in Figure 5a where the melting temperature and heat of fusion are 74.8 °C and 1.57 cal/g, respectively. When the BAMO component is 18%, the melting temperature and heat of fusion values are 69.5 °C and 0.28 cal/g, respectively (Figure 5b).

The thermogravimetric analysis (TGA) of the pure components as well as their blends exhibited the similar behaviour which is shown in Figure 6a. The TGA of the BAMO/AMMO (25% BAMO) material shown as an example in Figure 6a was carried out under N_2 atmosphere and the material totally degraded in the 240-260 °C range. This sharp degradation was observed for the two pure components as well as their blends when tested under 10 °C/min heating rate. However, when the heating rate was reduced to 1 °C/min, the extent of degradation decreased to 31% in the same

temperature range (Figure 6b). There was practically no degradation up to 200 °C for both heating rates.

BAMO/AMMO binder formulations were found to be highly flame resistant. These formulations, when subjected to flame at atmospheric conditions, burned slowly, and extinguished when the flame was removed.

SOLUBILITY OF THE POLYMERIC BINDER IN VARIOUS SOLVENTS

The solubility of the BAMO/AMMO polymeric binder in various solvents was tested by placing 0.03 g of the BAMO/AMMO(18%BAMO) sample in vials containing 5 ml of various solvents at 23 °C. The solution was not stirred. The polymeric binder was found to completely dissolve in ethyl acetate, tetrahydofuran (THF) and acetone. Swelling typically preceded dissolution. The polymeric binder did not dissolve in methanol and ethanol.

BAMO/AMMO(12%BAMO) and BAMO/AMMO(18%BAMO) polymeric binders were found to be highly soluble in ethyl acetate at ambient conditions. BAMO/AMMO(18%BAMO) polymeric binder formed a clear solution up to a concentration of about 20 wt.%. With increasing polymeric binder concentrations the solution became more viscous and yellowish in color. It took roughly 16 hours to form a single phase with 37 wt.% binder and 70 hours with 50 wt.% polymeric binder. For BAMO/AMMO (12%BAMO) polymeric binder, a single viscous phase was formed in 4 hours with 50 wt.% polymeric binder. With 60 wt.% polymeric binder it took 16 hours to form the single phase.

Based on the Fourier-transform Infrared (FTIR) analyses of the stock solutions containing varying amounts of the BAMO/AMMO polymeric binder dissolved in ethyl acetate, it was found that ethyl acetate has an IR absorbance peak at 2090 cm^{-1} which masks the azide peak of the binder at 2100 cm^{-1} for binder concentrations below 0.2 wt.%. Hence, for the low concentrations of the polymeric binder used in the dissolution experiments, IR spectra cannot be used when ethyl acetate is used as the solvent. However, the azide peak is not masked when THF is used as the solvent. Figure 7 is the calibration curve for determination of the polymeric binder concentrations in THF. Figures 8-10 illustrate the absorbance vs wavenumber spectra for pure THF, 3 minutes and 8 minutes after the beginning of the dissolution process, respectively. These figures illustrate the growing of the azide peak with time as the polymeric binder concentration in solution increases. The THF used was supplied by Aldrich, had a purity of 99+% and was inhibited with 0.025% butylated hydroxytoluene which may explain the interferences in the FTIR.

DISSOLUTION OF AMMONIUM SULFATE AND BINDER MIXTURES

In one set of experiments, ammonium sulfate (used as ammonium perchlorate simulant) was mixed with the BAMO/AMMO (12% BAMO) polymeric binder and ethyl acetate at room temperature to prepare a propellant simulant. Ethyl acetate was subsequently evaporated and the ammonium sulfate/polymeric binder mixture was placed in water in a shaker bottle. Upon mixing for about an hour at room temperature and at 90 °C, the amount of ammonium sulfate dissolved was determined by measuring ammonium ion concentration with an ammonium ion

specific electrode and was found to be insignificant. (The electrode calibration curve for determining ammonium sulfate concentrations are shown in Figure 11.) Since previous experiments demonstrated the high solubility of pure ammonium sulfate in water, it was concluded that the polymeric binder is forming a barrier to the solvation of ammonium sulfate by water.

When the simulant was contacted with a mixture of water and ethyl acetate (50 vol. % each) at room temperature, it was found to dissolve in approximately 10 minutes. Apparently the solvation of the binder by ethyl acetate makes ammonium sulfate accessible to water in which it is soluble. Ethyl acetate and water are not miscible and the cloudiness which results from their mixing prevents visual and camera monitoring of the dissolution process.

Although THF can solvate the binder just as effectively as ethyl acetate, a mixture of THF and water (50 vol.% each), which is miscible at room temperature, is incapable of solvating the simulant. Above 68 °C the mixture was found to form two phases, but again the solvent mixture did not dissolve the simulant. These results along with the color change of THF suggested that THF properties change upon mixing with water, adversely affecting its solvating ability.

In separate experiments at room temperature and 90 °C, the binder alone did not dissolve in THF-water mixture, however, ammonium sulfate alone did. This indicated that solvating ability of water for ammonium sulfate was not adversely affected upon mixing with THF.

EXPERIMENTAL SYSTEM FOR DISSOLUTION RATE EXPERIMENTS

The dissolution experiments were carried out using the experimental set-up shown in Figures 12a and 12b which illustrate a transparent vessel and an autoclave. The transparent vessel (Figure 12b) provided the opportunity the view and video record the progress of solvation. The transparent vessel which consists of a 500 ml pyrex bottle is heated electrically and equipped with a temperature controller. The agitation is achieved with a magnetic stirrer. The binder, approximately 0.3 g of BAMO/AMMO(12% BAMO), was shaped into a sphere and suspended at the end of a hooked wire in the transparent vessel. The solvent (THF) was heated and pressurized in an autoclave and was subsequently transferred to the transparent vessel in which agitation was achieved with a magnetic stirrer. Samples were collected at regular time intervals and analyzed by FTIR.

Since the binder is encapsulating other ingredients of the energetic formulations, binder dissolution rate data is of primary importance for rational design of equipment to recover the constituents of energetic materials. Such data should preferably be collected under temperature and flow conditions similar to the one expected in the commercial apparatus. Hence the primary objective of the dissolution rate experiments is to collect binder dissolution data and assess the affect of flow dynamics on the binder dissolution rates. This is best achieved using the autoclave shown in Figure 12a. The autoclave (Parr 4521) consists of one liter Hastelloy C vessel rated for 2000 psig and 350 °C. The autoclave is equipped with an impeller drive system, pressure gage, thermocouple and valve assembly to pressurize,

evacuate and take samples. The temperature and impeller speed are controlled by Parr 4842 PID controller.

In the autoclave, one can obtain better mixing and study the dissolution process for a wide range of Reynolds numbers corresponding to different impeller speeds. The anchor impeller was operated at speeds which provided much higher levels of agitation than was possible in the transparent vessel. Since the turbulence generated at high rotational speeds of the impeller resulted in the loosening of the binder from the hook used in the transparent vessel, measures were taken to hold the binder securely in a wire cage before suspending it in the autoclave.

MATHEMATICAL ANALYSIS OF THE DISSOLUTION PROCESS

Polymer dissolution phenomena in the literature have been primarily examined from the perspective of fabrication of integrated circuits and in controlled release applications. Early work [1] focused on the surface layer structure and identified the important parameters affecting the dissolution process. Numerous other studies emphasized the experimental methods to study polymer dissolution [2-5]. Theoretical studies were also carried out to develop mathematical models describing solvent diffusion in the polymer, polymer diffusion in the liquid layer adjacent to the polymer and the location of the solid-solvent interface [6] which also included the role of external mass transfer resistance [7]. Further theoretical development incorporated the polymer chain disentanglement mechanism into the relevant transport equations [8].

Typically, the dissolution of polymer does not take place immediately after contact with the solvent. A certain time period, called the "induction time", must elapse

before the polymer first dissolves into the solvent. The induction time depends on the nature of the polymer and solvent as well as the temperature. However, if the polymer is above its glass transition temperature which is the case for BAMO/AMMO, the induction time can be expected to be very small . Indeed in our experimental work the liquid samples collected in a very short time interval (within 30 seconds) after starting the dissolution process always contained a detectable amount of the dissolved polymer. This observation suggests that the film theory can be used to obtain mass transfer coefficients under different flow conditions. One can then predict the binder dissolution rates in a large scale operation which would enable rational scale-up effort.

The mathematical analysis for the dissolution process is based on the film theory for interfacial mass transfer [9]. Film theory assumes that a stagnant film the thickness of which depends primarily on the system hydrodynamics, exists near every interface. This hypothetical film also called the "unstirred layer" presumes that transport processes in the film occurs by diffusion alone with the concentration varying linearly across the thickness of the film. Since the film is assumed to be very thin, the quantity of solute within the film would be small relative to the amount passing through it so that a concentration gradient would be set up quickly. The molar flux of the solute across the film is then written as a product of mass transfer coefficient and the concentration difference across the film.

The film model is applied here to a specimen of spherical shape where the surface area A(t) is progressively shrinking. The molar diffusion flux of the solvated polymer in the film is given by

$$N = k (C_i - C_b) \qquad (1)$$

where N is the molar flux of the solute relative to the solid-fluid interface, k is the mass transfer coefficient and C_i and C_b are the interfacial and bulk concentrations in the fluid. Also, since the film is presumed to be very thin, there would be no mass accumulation in the film and the diffusional flux through the film (N) can be taken to be equal to the rate of dissolution (r_d) based on the external surface area A(t) of the dissolving particle and represented by

$$N \cdot M_w = r_d = -(1/A(t))dW_s/dt \qquad (2)$$

Here the molar flux (N) is multiplied by the molecular weight (M_w) of the binder to express the dissolution rate (r_d) in units of mass and W_s is the weight of the dissolving specimen. Hence Equation (2) states that the rate of decrease of the weight of the dissolving specimen per unit external surface area of the dissolving specimen is equal to the mass flux of the dissolving specimen through the film.

Combining Equations (1) and (2) and assuming that the interfacial concentration (C_i) will be equal to the equilibrium concentration (C_e) at the solid-liquid interface[9], one obtains

$$-(1/A(t))dW_s(t)/dt = kM_w(C_e - C_b) \qquad (3)$$

Here it will be assumed that the sphere retains its shape during dissolution and $C_b = 0$ at the low concentrations for which the data were collected. If the density of

the polymer during the dissolution process can be assumed to stay constant, then the surface area A(t) can be expressed in terms of the weight of the dissolving specimen ($W_s(t)$) and Eq. (3) can be integrated and (noting $W(t) = W_o - W_s(t)$) rearranged to yield

$$W(t)/W_o = 1 - (1 - k'W_o^{-1/3}\, t)^3 \qquad (4)$$

where $$k' = kC_eM_w(4\pi/3\rho^2)^{1/3} \qquad (5)$$

The parameters used in the above equations are as follows:

k = mass transfer coefficient

k' = constant defined by Eq. (5)

M_w = molecular weight of the dissolving polymer

N = molar flux of the dissolving polymer

t = time

$W_s(t)$ = weight of the polymer at time t

W(t) = weight of the dissolved polymer in solution at time t

C_e= concentration of the dissolved polymer in solution in equilibrium with with the solid polymer

W_o = initial weight of the polymer particle

ρ = density of the polymer

One would note that Eq. (4) should be used up to $t = W_o^{1/3}/ k'$ at which time all of the polymer will have dissolved in the solution. Also C_e is treated as constant with the assumption that solubility is not significantly influenced in the temperature range at which the data were collected.

RESULTS AND DISCUSSION

a) Dissolution Data Obtained with the Transparent Vessel

Figures 13 and 14 summarize the dissolution experiments in the temperature range of 34 - 67 °C. These plots show the fraction of the binder dissolved into the solution as a function of time. The weight of the binder dissolved into the THF solution were calculated by using the calibration curve (Figure 7) where the absorbance peak height values of the azide at 2100 cm^{-1} are plotted as a function of binder concentration in solution. The curves obtained from the best fit by using non-linear regression analysis based on Eq. (4) are also shown in Figures 13 and 14 and illustrate satisfactory fit to the data.

Since the dissolution rate as expressed by the LHS of Eq. (3) is based on the external surface area and that the RHS of Eq. (3) is constant at a fixed temperature, one would expect that the amount of binder which has dissolved into the solution at subsequent time intervals decrease in the same proportion as the external surface area. Figures 13 and 14 which plot the fraction of binder dissolved into the solution as a function of time clearly illustrate that the increase of the dissolved binder content in solution is decreasing with time.

The non-linear regression analysis using Eq. (4) yielded, as expected, increasing values of k' (a modified form of mass transfer coefficient (or dissolution rate constant) defined by Eq. (5)) corresponding to each temperature. The data given in Figures 13 and 14 were also used to calculate the diameter of the dissolving spherical polymeric binder at any given time (assuming the binder retained its shape during dissolution). By expressing the surface area and weight of the dissolving specimen on the LHS of Eq. (3) in terms of the diameter, it becomes apparent that the diameter of the dissolving binder will be decreasing linearly with time. Hence linear regression was carried out and k' were calculated using a version of Eq. (4) expressing diameter as a function of time. The k' obtained by both methods were found to be essentially identical confirming the accuracy of the numerical techniques.

The k' obtained at different temperatures were plotted as a function of temperature in the Arrhenius form in Figure 15. The activation energy was found to be 4.6 kcal/mol which is typical for diffusion controlled processes. Figure 15 shows that ln(k)' vs 1/T plot is not quite linear, higher temperature data indicating lower activation energy. One possible explanation for this observation is the differences in the activation energies associated with internal diffusion (i.e. diffusion of the solvent into the polymer) and external diffusion (i.e. diffusion of the solvated polymer from the polymer-solvent interface into the bulk solvent) which both affect the overall rate of dissolution with the external diffusion having, in general, a lower activation energy than internal diffusion. Hence, the implication here is that contribution of external diffusion to the overall dissolution rate is becoming more important at higher temperatures. The relaxation of the constant solubility assumption would not account for the lowering in the activation energy since solubilities are expected to increase

with temperature which would mean that based on this effect alone, one would observe an increase in k' values (or activation energies) at the higher temperatures rather than the decrease observed here.

The experiments performed here were at the highest level of agitation provided by the magnetic stirrer of the transparent vessel which apparently did not eliminate external mass transfer resistance. To minimize the external mass resistance more effective agitators need to be used as we have done in conjunction with the autoclave reactor the results of which will be given in the next section. The transparent vessel affords the capability to monitor the solid-fluid boundary with a video, revealing how the flow dynamics affect the dissolution rates. We were able to observe that the surface of the polymer upon which the circulated solvent directly impinged, dissolved at an accelerated pace. However, since the hydrodynamic conditions were not uniform around the polymer surface, the polymer particle did not strictly retain its spherical shape (Figure 16). Although Figure 16 does not give any indication of the velocity field around the polymer sample, the direction and intensity of the velocity field is discernible from the video observation where the increase in the local rate of dissolution was evident when the solvent directly impinged on the binder. It was also observed that the dissolution rate was very slow when there was no agitation. The solvated polymer was observed to be dragging down along the sides of the binder forming long strips at the bottom, which thinned out and eventually disappeared into the solution.

b) Dissolution Data Obtained with the Autoclave

The dissolution rate data in the autoclave at different impeller speeds are given in Figure 17. Impeller speeds of 100- 400 RPM would correspond to a Reynolds number range of $1.5x10^4$ - $6.1x10^4$. Here the Reynolds number is defined as $\rho ND^2/\mu$, where N is the RPM, D is the distance between impeller tips and ρ and μ are the density and viscosity of the solution respectively.There is a significant increase in the amount of binder dissolved at any given time when the impeller speed is increased from 100 RPM to 200 RPM. This implies significant external mass transfer resistance at the low Reynolds number which can also be interpreted as the region of high sensitivity of the mass transfer coefficient (k) on the Reynolds number.

The curves obtained from non-linear regression analysis by using Eq. (4) are also shown in Figure 17 with the accompanying k' values at different impeller speeds. One observes that as the Reynolds number changes from $1.5x10^4$ to $3.0x10^4$, the k' value essentially doubles. However, for further increases in the impeller speed, the corresponding increases in k' are less. For instance when the Reynolds number increases from $4.5x10^4$ to $6.1x10^4$, the corresponding increase in k' is only 4%. This indicates that the rate controlling step has changed from external mass transfer i.e., diffusion of dissolved binder into the bulk liquid phase, to diffusion of solvent into the binder.

The hydrodynamic conditions obtained with the magnetic stirrer in the transparent vessel would correspond to the low RPM range in the autoclave agitated with an anchor impeller. For example, the k' value obtained for the transparent vessel at 17°C is 0.013 $g^{1/3}min^{-1}$ which is 13% lower than the k' value calculated at 100RPM in the autoclave at the same temperature. This confirms that the external mass transfer

temperature range of 21°C to 60°C. The agitation level was kept at 400 RPM to keep the effect of external mass transfer resistance to a minimum. The results are illustrated in Figure 18 with the curves (and the corresponding experimental k' values) obtained on the basis of the best fit using Eq. (4). Figure 19 shows the Arrhenius plot of the k' values calculated at different temperatures. The activation energy of 4.8 kcal/mol is remarkably close to 4.6 kcal/mol obtained on the basis of data collected using the transparent vessel indicating the effect of the external mass transfer in the transparent vessel on the calculated activation energy is not significant. Moreover, ln(k') vs 1/T plot based on the data collected in the autoclave is essentially linear. This is consistent with the observation that the nonlinearity of ln(k') vs 1/T plot for the data collected in the transparent vessel was primarily due to the presence of external mass transfer which is essentially eliminated in the autoclave reactor due to much higher levels of agitation with the anchor stirrer.

ACKNOWLEDGEMENT

Office of Naval Research is gratefully acknowledged for supporting this work under the contract N-00014-95-1-0770.

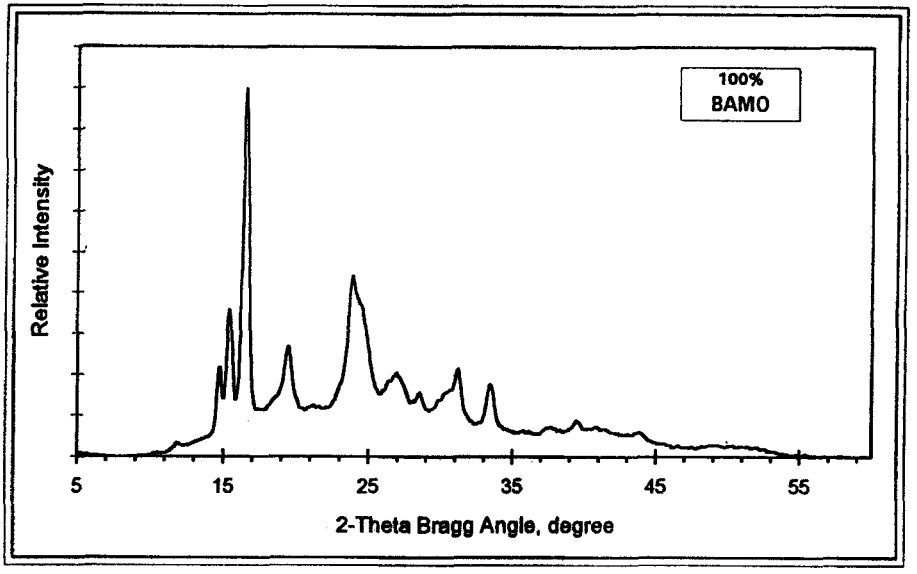

Figure 1. WA-XRD pattern of pure BAMO

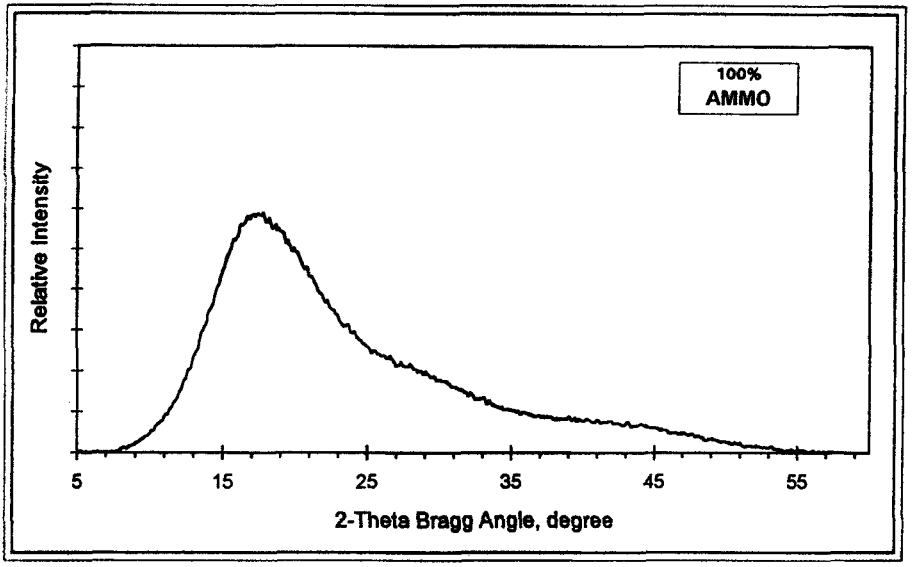

Figure 2. WA-XRD pattern of pure AMMO

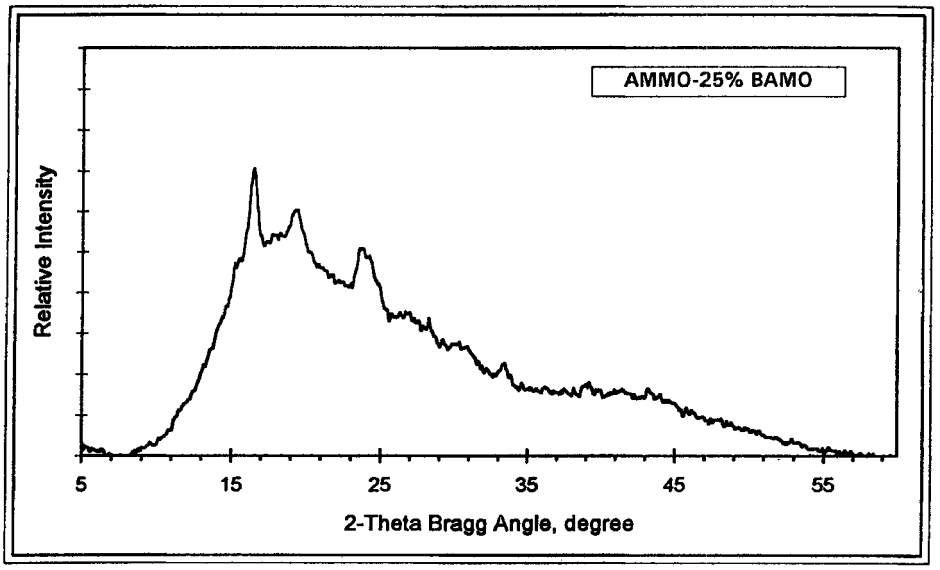

Figure 3a. WA-XRD pattern of AMMO-25%BAMO

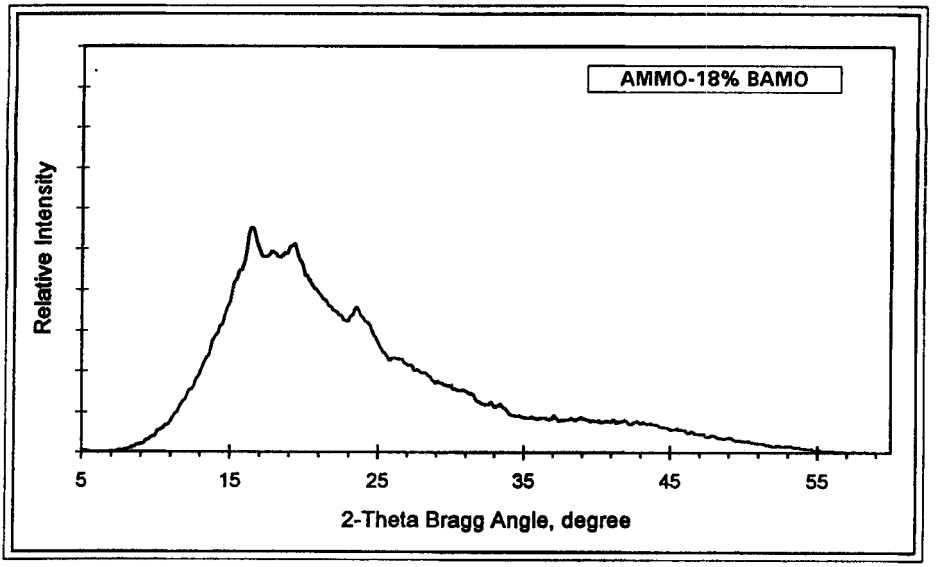

Figure 3b. WA-XRD pattern of AMMO-18%BAMO

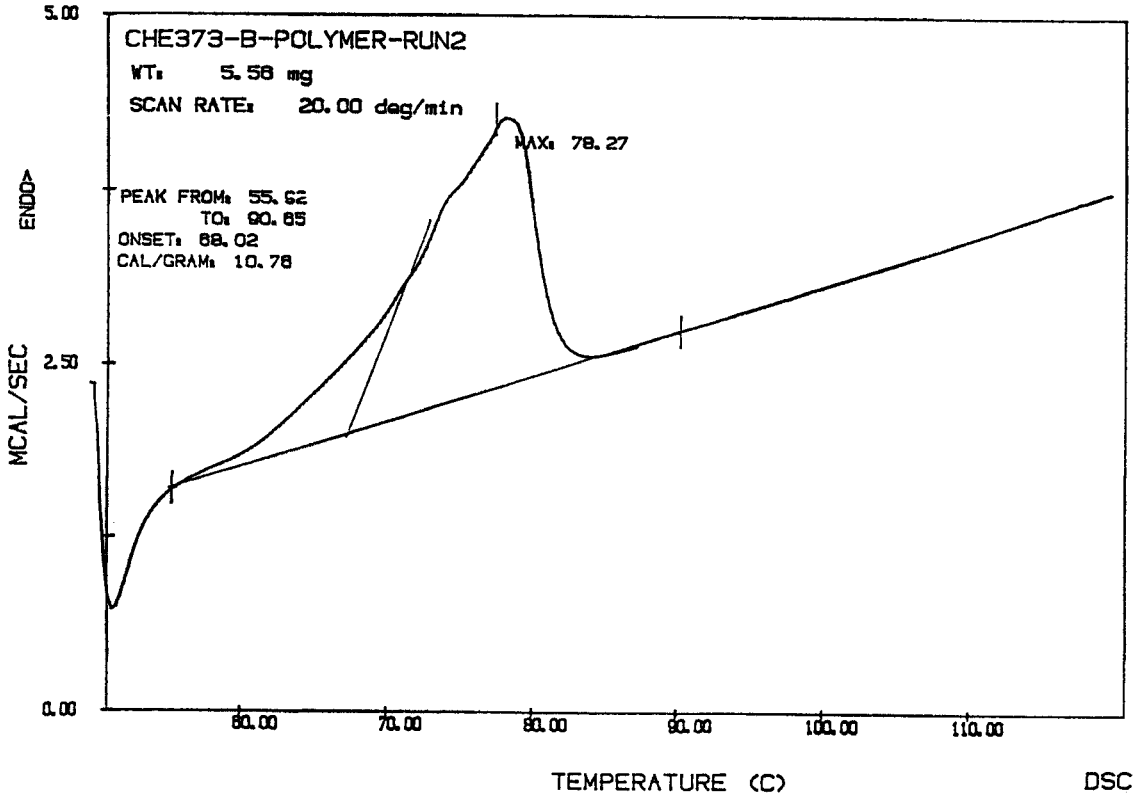

Figure 4. DSC of pure BAMO

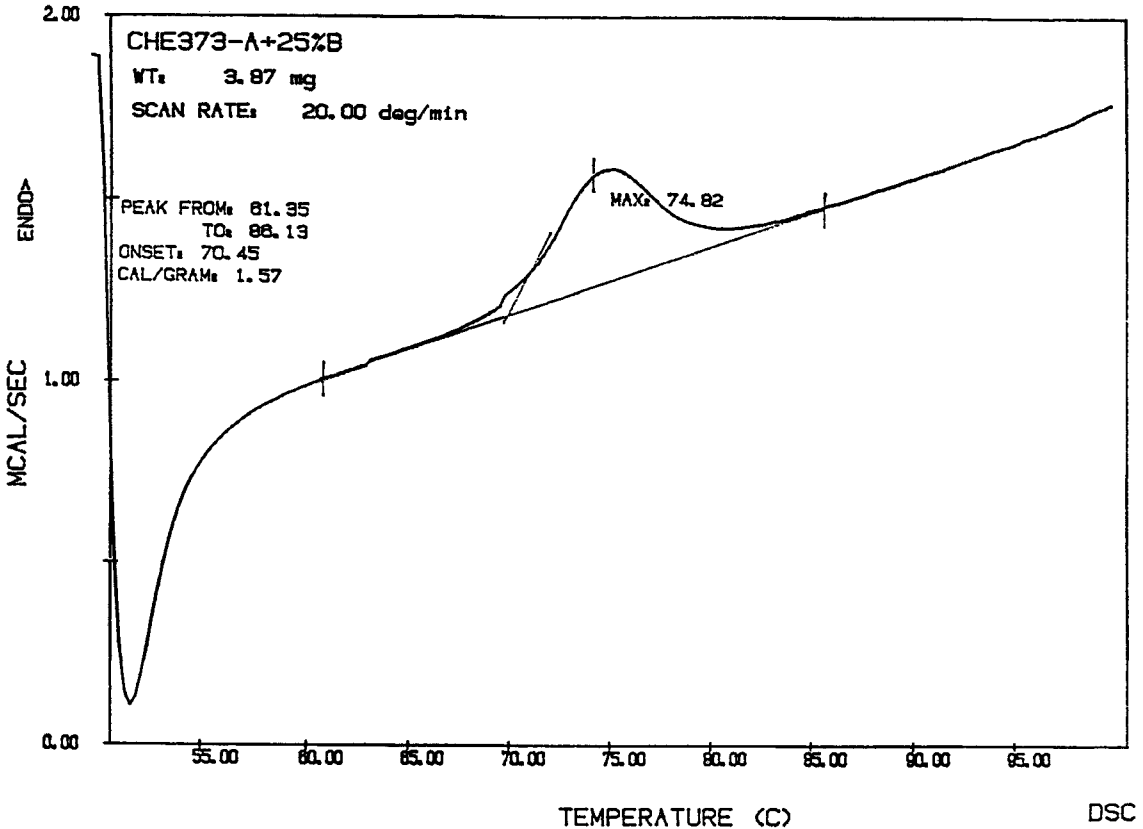

Figure 5a. DSC of AMMO - 25% BAMO

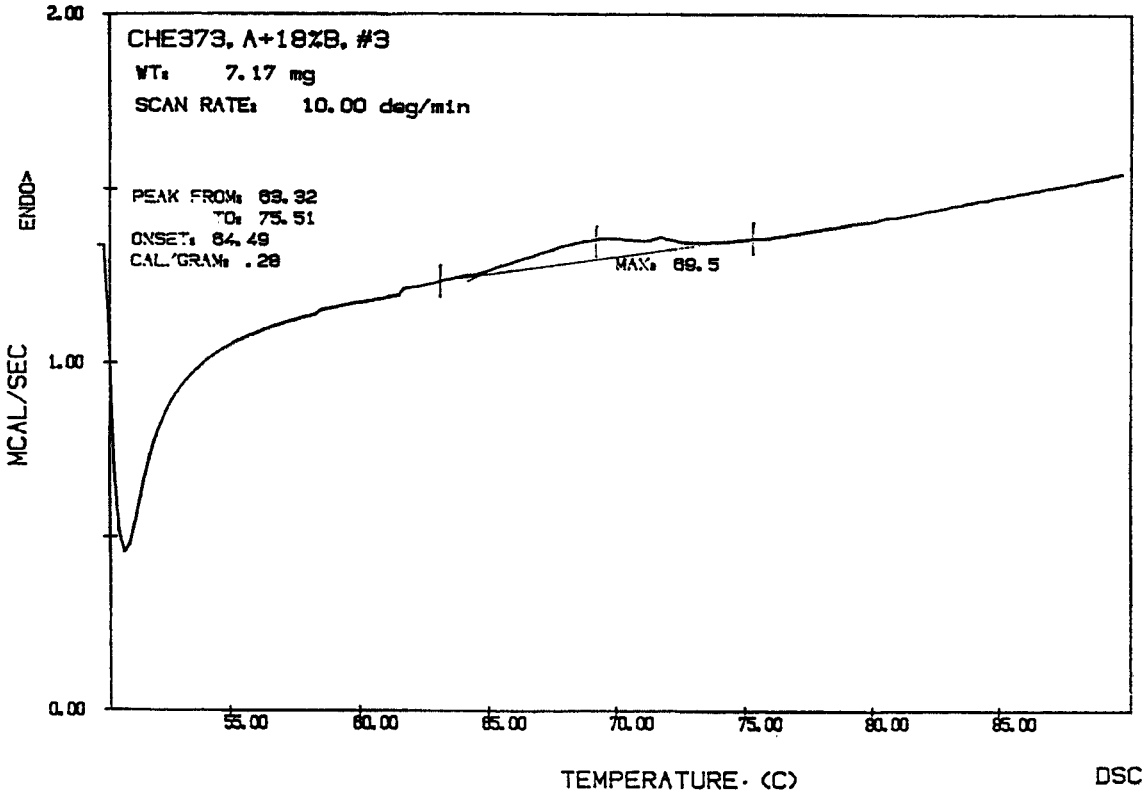

Figure 5b. DSC of AMMO - 18% BAMO

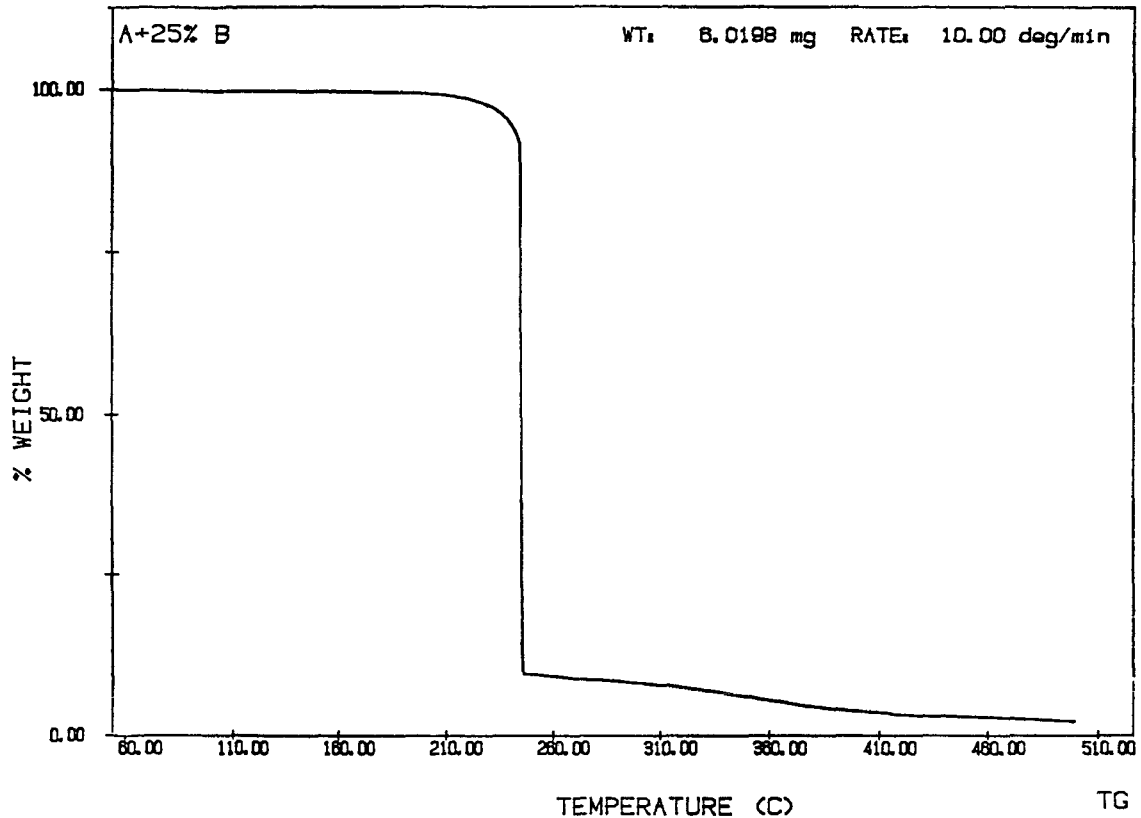

Figure 6a. TGA of AMMO - 25% BAMO with 10 °C/min heating rate.

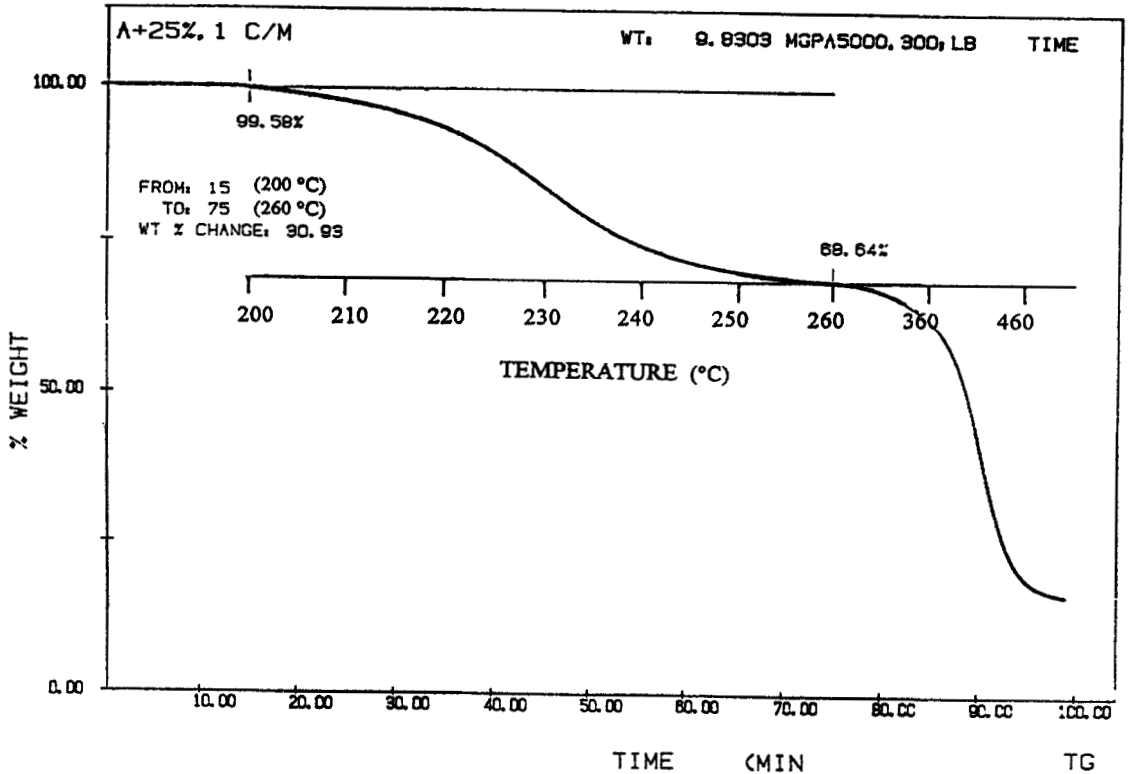

Figure 6b. TGA of AMMO - 25% BAMO with 1 °C/min heating rate.

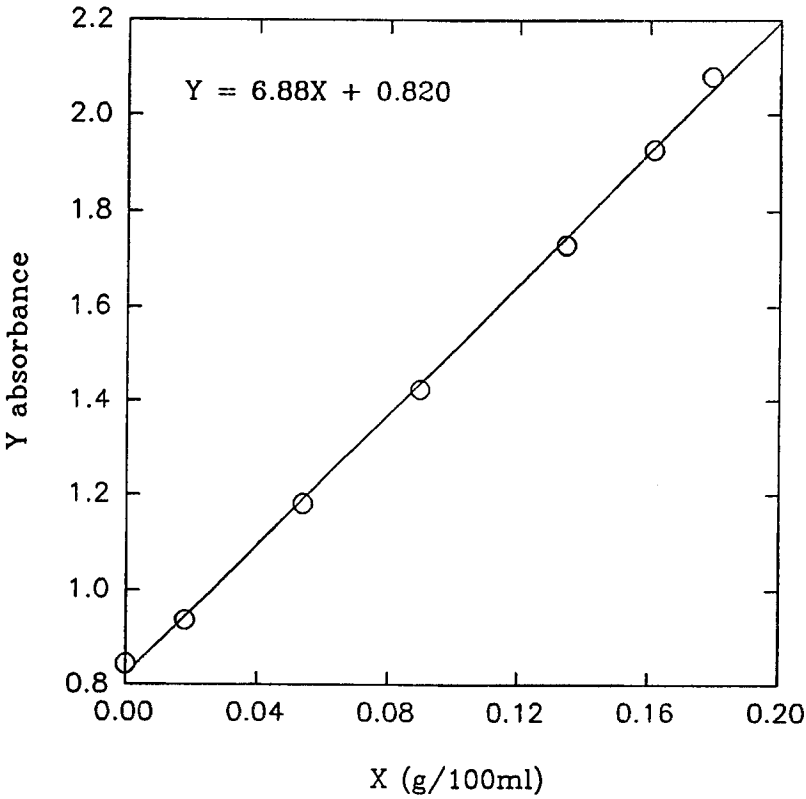

Figure 7: Calibration Curve
FTIR Absorbance vs. Concentration

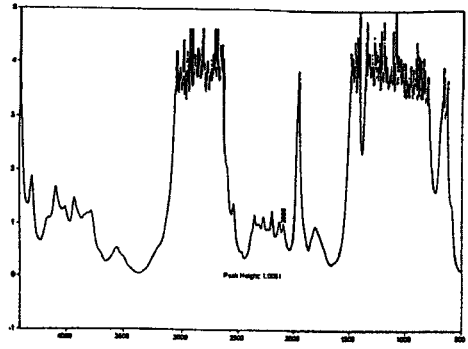

Fig. 8: FTIR Spectra of Pure THF (Absorbance vs. Wavenumber, cm^{-1})

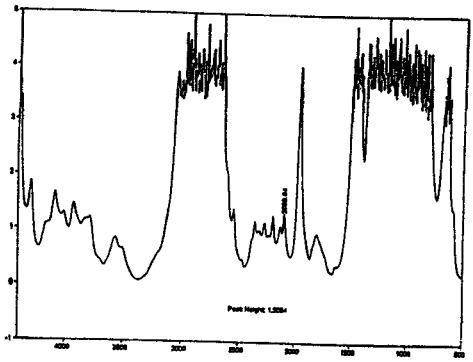

Fig. 9: FTIR Spectra of BAMO/AMMO in THF after 3 min (Absorbance vs. Wavenumber, cm^{-1})

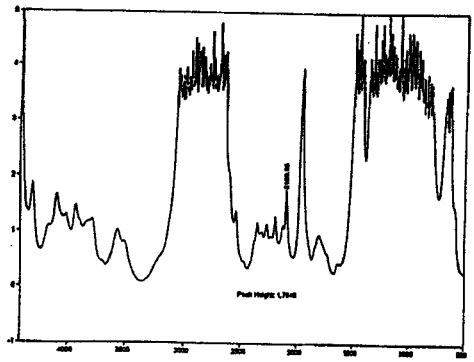

Fig. 10: FTIR Spectra of BAMO/AMMO in THF after 8 min (Absorbance vs. Wavenumber, cm^{-1})

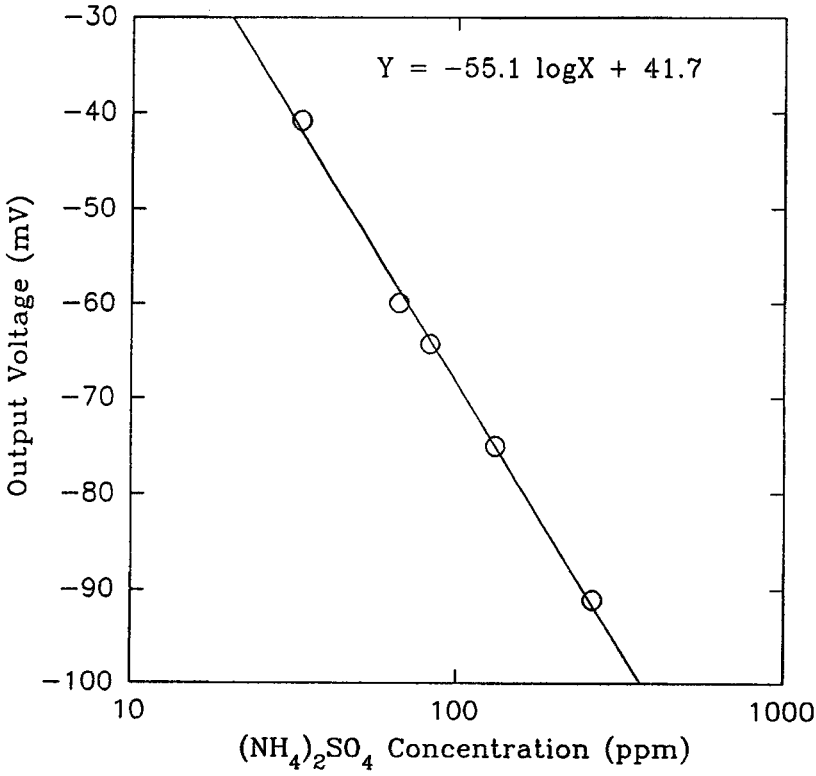

Figure 11: Calibration Curve
Output Voltage vs. Concentration

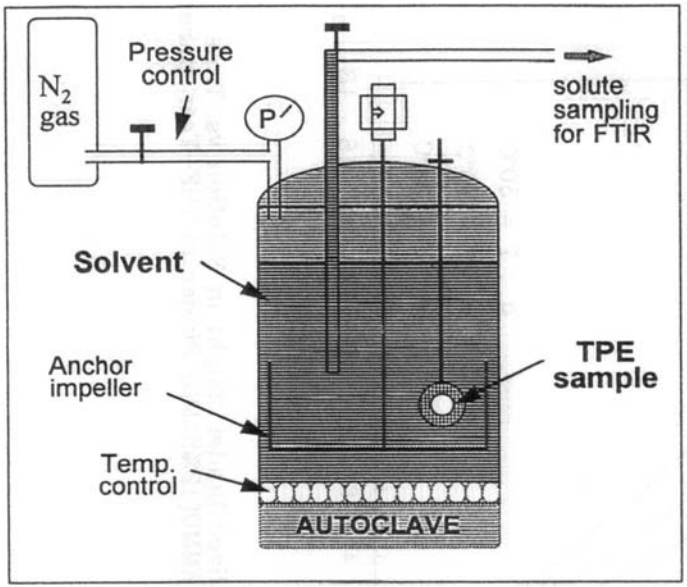

Figure 12a. Autoclave setup for dissolution rate and flow dynamics analysis

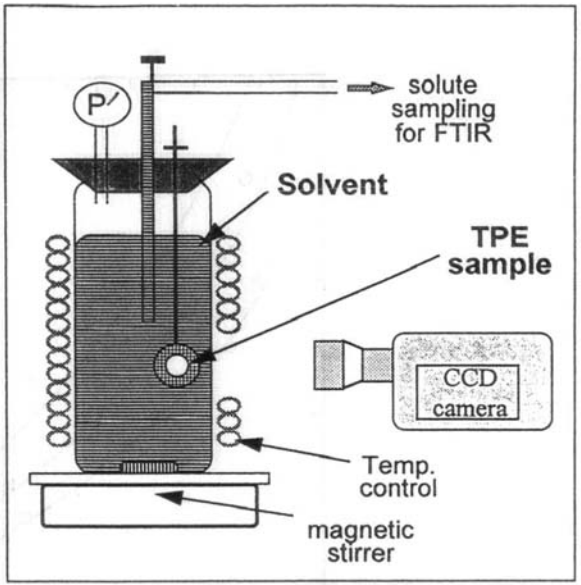

Figure 12b. Transparent dissolver setup for dissolution rate and visual analysis

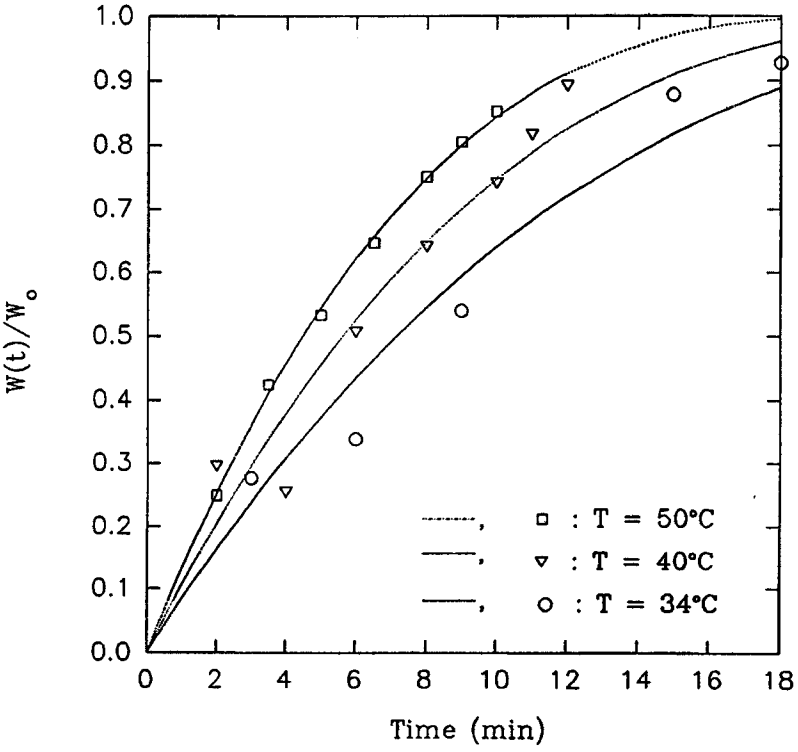

Figure 13: Normalized Binder Weight in Solution vs. Time
BAMO/AMMO(12%BAMO) Binder in THF–Transparent Vessel

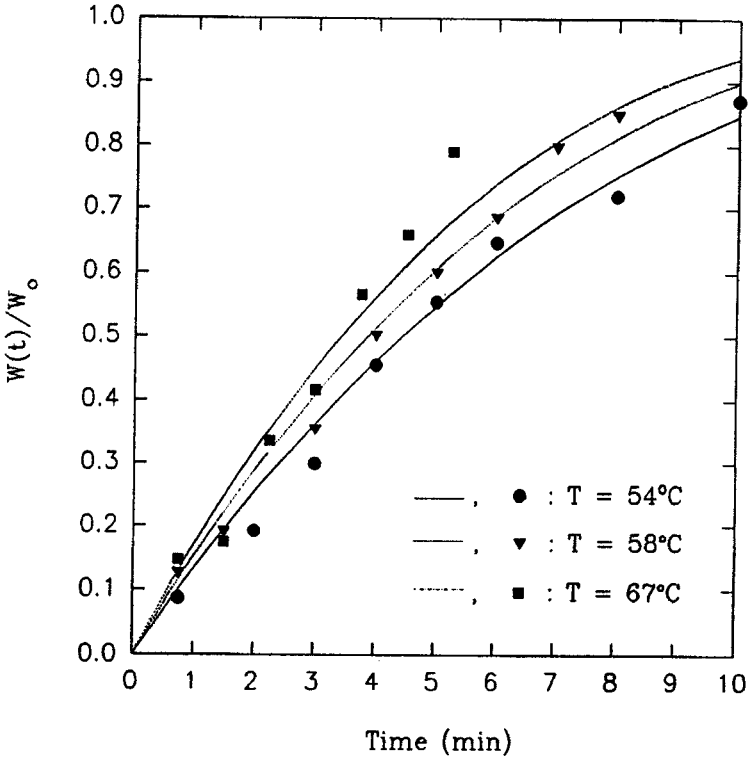

Figure 14: Normalized Binder Weight in Solution vs. Time
BAMO/AMMO(12%BAMO) Binder in THF–Transparent Vessel

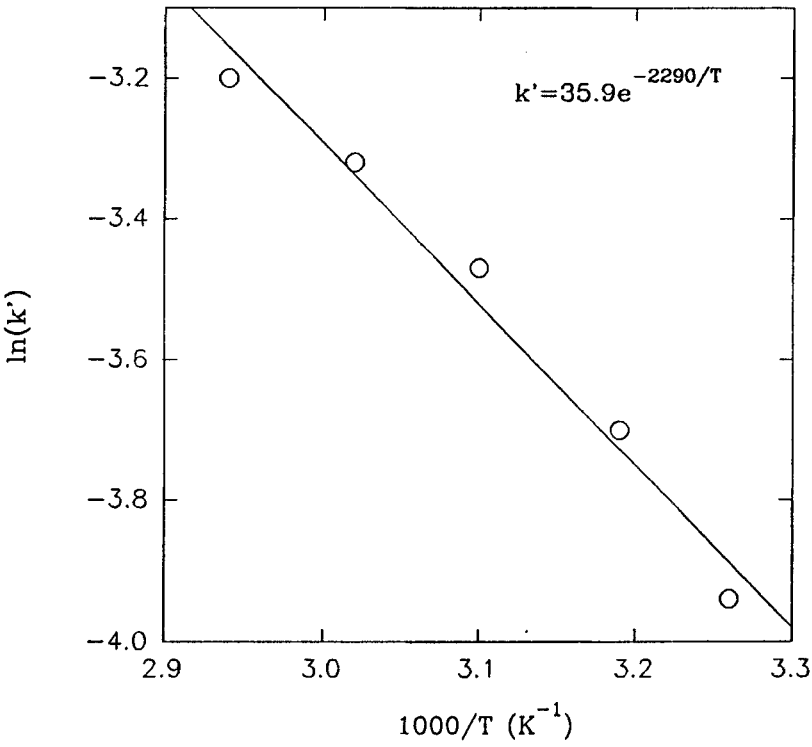

Figure 15: Arrhenius Plot–Transparent Vessel

(a)

(b)

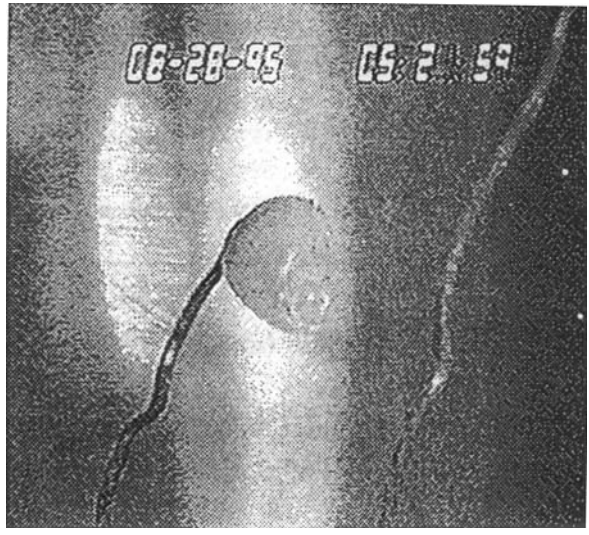

Figure 16: Dissolution of BAMO/AMMO in THF
(a) beginning of dissolution
(b) after180 seconds of dissolution

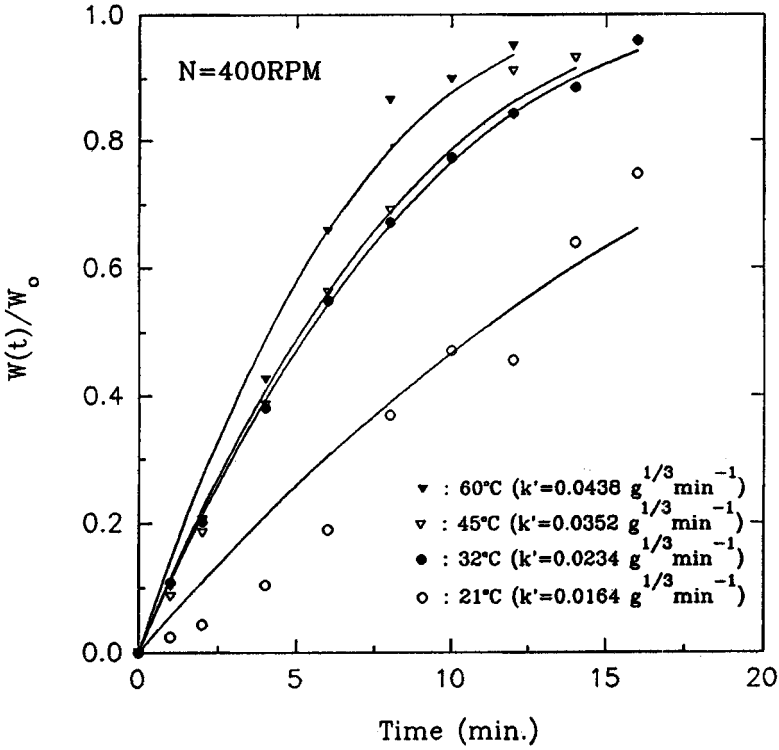

Figure 18: Normalized Binder Weight in Solution vs. Time BAMO/AMMO(25% BAMO) Binder in THF–Autoclave

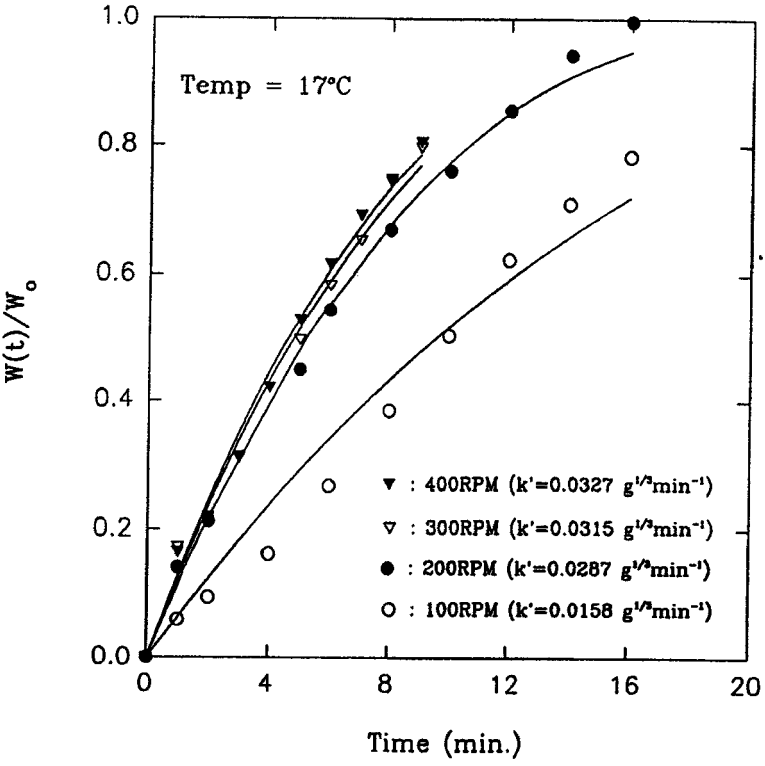

Figure 17: Normalized Binder Weight in Solution vs. Time BAMO/AMMO(12%BAMO) Binder in THF–Autoclave

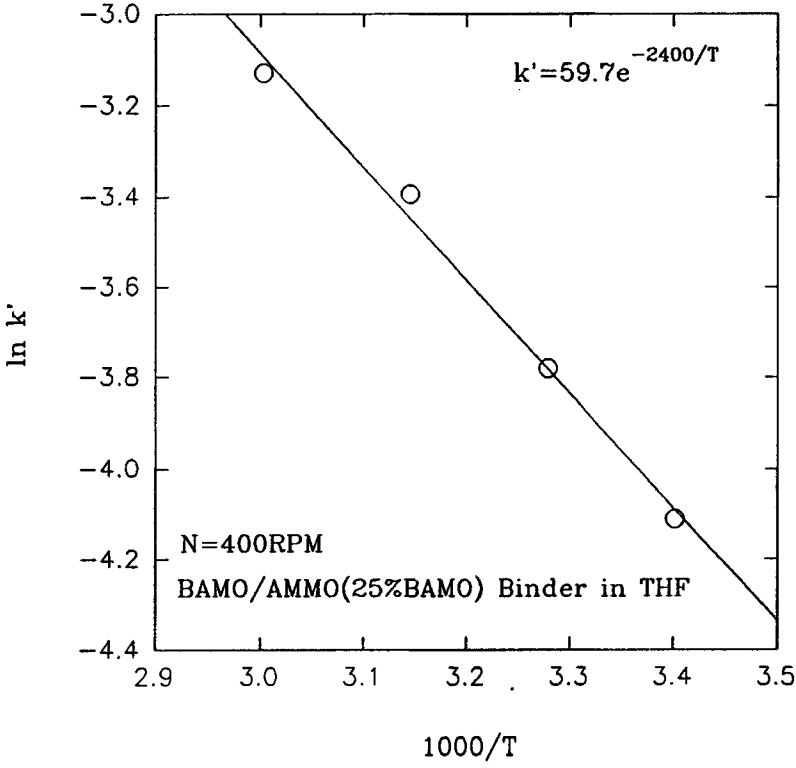

Figure 19: Arrhenius Plot–Autoclave

REFERENCES

1. K. Ueberreiter, in "Diffusion in Polymers", J. Crank and G.S. Park, eds., Academic Press, NY, 1967.

2. A. C. Ouano, Polymer Eng. & Sci., Vol. 18, No. 4, 306 (1978).

3. A. C. Ouano and J.A. Carothers, Polymer Eng. & Sci., Vol. 20, No. 2, 160 (1980).

4. W. J. Cooper, P. D. Krasicky and F. Rodriguez, J. of Applied Polymer Sci., Vol. 31, 65 (1984).

5. F. Rodriguez, P.D. Krasicky and R. J. Groele, Solid State Technology, May, 125 (1985).

6. O. Y. Tu and A. C. Ouano, IBM J. Res. Dev., Vol. 6, 207 (1987).

7. P. I. Lee and N. A. Peppas, J. Controlled Release, Vol. 6, 207 (1987).

8. N. A. Peppas, J. C. Wu and E. D. Meerwall, Macromolecules, Vol. 27, 5626 (1994).

9. R. E. Treybal, "Mass Transfer Operations", McGraw Hill, New York, 1987.